HHS Public Access

Author manuscript

Small. Author manuscript; available in PMC 2019 March 04.

Published in final edited form as:

Small. 2014 April 09; 10(7): 1245–1249. doi:10.1002/smll.201303263.

Fe_5C_2 Nanoparticles with High MRI Contrast Enhancement for Tumor Imaging

Wei Tang,
Department of Chemistry and Bio-Imaging, Research Center (BIRC), University of Georgia, Athens, GA, 30602, USA

Dr. Zipeng Zhen,
Department of Chemistry and Bio-Imaging, Research Center (BIRC), University of Georgia, Athens, GA, 30602, USA

Ce Yang,
Department of Materials Science and Engineering, College of Engineering, Peking University, Beijing, 100871, China

Luning Wang,
Department of Physics and Astronomy, and Bio-Imaging Research Center, University of Georgia, Athens, GA, 30602, USA

Taku Cowger,
Department of Chemistry and Bio-Imaging, Research Center (BIRC), University of Georgia, Athens, GA, 30602, USA

Dr. Hongmin Chen,
Department of Chemistry and Bio-Imaging, Research Center (BIRC), University of Georgia, Athens, GA, 30602, USA

Trever Todd,
Department of Chemistry and Bio-Imaging, Research Center (BIRC), University of Georgia, Athens, GA, 30602, USA

Dr. Khan Hekmatyar,
Bio-Imaging Research Center, University of Georgia, Athens, GA, 30602, USA

Prof. Qun Zhao,
Department of Physics and Astronomy, and Bio-Imaging Research Center, University of Georgia, Athens, GA, 30602, USA

Prof. Yanglong Hou, and
Department of Materials Science and Engineering, College of Engineering, Peking University, Beijing, 100871, China

Prof. Jin Xie

Supporting Information
Supporting Information is available from the Wiley Online Library or from the author.

Department of Chemistry and Bio-Imaging, Research Center (BIRC), University of Georgia, Athens, GA, 30602, USA

Stable colloidal nanoparticles with strong magnetization have attracted much attention for their great potential in biomedical applications.[1] In particular, they can be used as contrast probes in magnetic resonance imaging (MRI) by inducing hypo-intensities on T_2 and T_2*-weighted MRI maps. [2] So far, the most commonly used MRI contrast agents are iron oxide nanoparticles. However, due to moderate magnetization (~8 0 emu/g for Fe_3O_4 and ~70 emu/g for Fe_2O_3), [1a,3] iron oxide nanoparticles as MR probes suffer from suboptimal contrast enhancement. r_2 relaxivity, the measure of contrast ability, is ~100 $mM^{-1}s^{-1}$ for Feridex[1a], a clinically used iron oxide formula, and is ~200 $mM^{-1}s^{-1}$ for iron oxide nanoparticles made from more advanced synthetic approaches. [4] To exceed this limit, efforts have been made to fabricate nanoscale particles with even higher magnetization. For instance, Fe,[5] CoFe,[6] Co,[7] FePt,[8] and $SmCo_5$[9] nano-particles have been recently prepared by us and others via wet chemistry routes. Translation of these nanoparticles into biomedical practices, however, has encountered difficulties of various sorts. For instance, Fe, Co, and CoFe are very reactive at ambient conditions, and are susceptible to rapid oxidization and magnetism loss. [5–7] FePt and $SmCo_5$ nanoparticles need to be annealed at high temperature to be granted with high magnetism. However, the annealing process is accompanied with severe particle aggregation. [9a, 10] More critically, most of these nanoparticles are associated with high toxicity that limits their wide use in biological settings. [8b, 11]

Iron carbides (Fe_3C, Fe_5C_2, and Fe_7C_3), used primarily in metallic alloys and hard coatings, are one of the most ancient materials in human history. Iron carbides are also known to possess appealing magnetic properties. Fe_5C_2 for instance, has a magnetic moment of ~ 140 emu/g, [12] a value that is comparable to that of Co (~1 60 emu/g) and two times higher than that of Fe_3O_4. Unlike Co or Fe, iron carbides boast good chemical stability, and hence are largely immune to oxidization-induced magnetization drop. Such strong and stable magnetism suggests their potential applications in biomedicine. The related exploits, however, have seldom been attempted. The main challenge comes from the difficulty of preparing nanoparticulate iron carbides. Conventionally, iron carbides are made at high-temperatures and in reducing conditions, [13] which are hard to replicate in a laboratory setting. There have been reports on utilizing laser pyrolysis [14] and high temperature sol-gel methods to prepare iron carbide nanoparticles. [13,15] The products, however, do not afford the size and/or colloidal stability that are desired for bio-medical applications.

A breakthrough by us recently allowed one to prepare Fe5C2 nanoparticles by a facile and mild wet-chemistry route.[12] The products possess close-to-bulk magnetization, small and tunable particle size (<25 nm), narrow size distribution, and good colloidal stability. Following this success, we herein evaluated the potential of Fe_5C_2 nanoparticles as a MR contrast probe, which, to the best of our knowledge, is the first time. We found that Fe_5C_2 nanoparticles, after surface modification with phospholipids, could be stably dispersed in aqueous solutions (Scheme S1). The particles displayed an r_2 relaxivity of 464.02 $mM^{-1}s^{-1}$, which is among the highest of all MR probes reported. When coupled to a tumor targeting

ligand, Fe_5C_2 nanoparticles were able to home to tumors and induce more prominent signal change than Fe_3O_4 nanoparticles. These observations strongly suggest the great promise of Fe_5C_2 in MR imaging as well as in other biomedical fields.

We followed our reported protocol to prepare Fe_5C_2 nanoparticles.[12] Briefly, a mixture of octadecylamine and cetyltrimethyl ammonium bromide (CTAB) was rigorously stirred and degassed under argon. The solution was heated to 393 K, at which time $Fe(CO)_5$ was injected. The resulting mixture was further heated to 453 K and kept at the temperature for 10 min. Finally, the temperature was increased to 623 K and kept for 10 min before cooling to room temperature. The nanoparticles were purified with ethanol and redispersed in hexane. Transmission electron microscope (TEM) analysis showed that the nanoparticles are comprised of a Fe_5C_2 core (~19 nm) and a Fe_3O_4 shell of ~2 nm[12], and the overall particle size was around 23 nm (Figure 1a). The magnetism of the particles was studied by a SQUID magnetometer. A saturation magnetization (Ms) of ~125.4 emu/g was observed at room temperature (Figure 1b, black curve), which is close to the bulk materials'. This value is also among the highest reported with colloidally stable nanoparticles, compared to that of ~7 0 emu/g for iron oxide nanoparticles,[16] ~100 emu/g for Fe nanoparticles,[5] and ~115 emu/g for Co nanoparticles.[7] Notably, the particles showed no remnant magnetization or coercivity at room temperature, i.e. they are superparamagnetic. This ensures good particle dispersibility that is critical to their uses in a biological context. Another important feature is that the particles are very stable in the air. After one week aging in air the Fe_5C_2 nanoparticles showed an almost unchanged hysteresis loop (Figure 1b, red curve).

The as-synthesized Fe_5C_2 nanoparticles are coated with a layer of octadecylamine and are hydrophobic. To render them water soluble, we imparted a phospholipid derivative, 1,2-distearoyl-sn-glycero-3-phosphoethanolamine-N[carboxy(polyethylene glycol)-2000] (DSPE-PEG-COOH), onto the particle surface. DSPE-PEG-COOH is an amphiphilic compound. It immobilizes on the particle surface through hydrophobic-hydrophobic interactions between its alkyl chains and the octadecylamine coating. The PEGylated, hydrophilic section faces outward, interacting with the aqueous surroundings to afford the particles with good dispersibility. The particles are stable in water, PBS, and serum (Figure S1). Figure 1c is a TEM image of DSPE-PEG-COOH coated nanoparticles in water. There is a dim halo (pointed by red arrows) surrounding each nanoparticle, which is attributed to the phospholipid coating. The dynamic light scattering (DLS) results were well correlated with the TEM observations, finding average sizes of 22 and 35 nm (Figure 1d) for particles before and after the surface coating, respectively.

We next assessed the r_2 relaxivity of these phospholipid-coated Fe_5C_2 nanoparticles. Briefly, we suspended Fe_5C_2 nanoparticles at a concentration gradient (0.05, 0.1, 0.25, 0.5, and 1 μg Fe/mL) in 1% agarose gel. We then subjected these gel samples to MR scans on a 7.0 T magnet using T_2 -weighted fast spin-echo sequences of different TEs. As a comparison, Fe_3O_4 nanoparticles (from Ocean Nanotech, Springdale, AR) samples at the same Fe concentrations were also prepared and scanned. While both sets of samples showed concentration dependent signal drop (Figure 2a), Fe_5C_2 nanoparticles induced greater hypo-intensities at the same concentrations. The linear fitting shown in Figure 2b indicates that the r_2 relaxivity of the Fe_5C_2 nanoparticles is 464.02 $mM^{-1}s^{-1}$, which is ~2.6 times higher than

that of Fe_3O_4 nanoparticles (178.30 $mM^{-1}s^{-1}$). This value is among the highest of all the MR probes reported.

As a novel nanomaterial for bio-related applications, a primary concern is toxicity. This was studied by (3-(4,5-dimethylthiazol-2-yl)-2,5-diphenyltetrazolium bromide (MTT) assays with U87MG (human glioblastoma) cells. Within the tested range (0–25 μg Fe/mL), U87MG cells retained over 80% viability over 24 h, indicating good tolerance to the Fe_5C_2 nanoparticles (Figure 3a). The cytotoxicity was also studied by live/dead assays (Invitrogen), where green (calcein AM) and red (ethidium homodimer-1) fluorescence mark live cells and dead cells, respectively. The outcomes were consistent with the MTT results, finding no substantial cell death when the particle concentration was below 25 μg Fe/mL (Figure 2b). Notably, though a small amount of CTAB was used as a precursor in the synthesis, none remained on yielded Fe_5C_2 nanoparticles, as confirmed in our previous studies.[12]

The multiple carboxyl groups on the particle surface allow for easy coupling with biomolecules. For a proof-of-concept study, we coupled a peptide, c(RGDyK), onto the Fe_5C_2 nanoparticles (Scheme S1). c(RGDyK) is an RGD derivative with high affinity towards integrin $\alpha_v\beta_3$ that is overexpressed on tumor vasculature and tumor cells of various types.[17] The coupling was mediated by 1-ethyl-3-(3-dimethylaminopropyl) carbodiimide (EDC) and sulfo-(N-hydroxysulfosuccinimide) (NHS), and the particles were collected and purified using a microcon centrifugal filter unit (YM-100, Millipore). The final products, c(RGDyK)-conjugated Fe_5C_2 (hereafter referred to as RGD-Fe_5C_2), were dispersed in PBS. No substantial aggregation was observed during the coupling and purification processes.

The targeting specificity was first assessed in vitro with U87MG cells, which are integrin $\alpha_v\beta_3$ positive. Briefly, RGD-Fe_5C_2 nanoparticles (5 αg Fe/mL) were incubated with fixed U87MG cells for 1 h. After removing the solution, the cells were washed with PBS and subjected to Prussian blue staining to reveal the Fe distribution. Almost all of the cells were positively stained, suggesting good particle uptake (Figure 3c). In contrast, when non-targeting Fe_5C_2 nano-particles (not conjugated with the c(RGDyK)) were used, there was a much lower level of cellular uptake. The results confirm that the particle targeting and uptake were mainly mediated by RGD-integrin interactions.

With the encouraging phantom and in vitro data, we next evaluated the particles in vivo in U87MG tumor bearing mice (n = 3). The animal model was established by subcutaneously injecting approximately 5×10^6 U87MG cells into the right hind limb of each mouse. In vivo MR imaging was conducted when the tumor size reached about 200–500 mm^3, at which time RGD-Fe_5C_2 or Fe_5C_2 nanoparticles were intravenously administered at a dose of 10 mg Fe/kg. A similar dose was used by us and others in previous investigations with Fe_3O_4 nanoparticles.[18] For comparison, Fe_3O_4 nanoparticle (20 nm, from Ocean Nanotech) and c(RGDyK) conjugates (RGD-Fe_3O_4 were injected at the same dose.) T_2-weighted MR images were acquired before, and 4 and 24 hours after the particle injection (Figure 4a). In the RGD-Fe_5C_2 group, significant signal drop in the tumor areas was observed at both 4 and 24 h time points, manifested as unevenly distributed black spots (pointed by red arrows). This distribution pattern is a reflection of the tumor heterogeneity,

and is consistent with the observations made by us[18b] and others[19] previously. On the contrary, little signal change was visualized in the control group, where Fe_5C_2 nanoparticles were injected. RGD-Fe_3O_4 also induced hypointensities in tumors but the signal change was not as dramatic as that with RGD-Fe_5C_2. By choosing signals in the leg muscle as a reference, we compared the relative intensity change. Compared to RGD-Fe_3O_4, RGD-Fe_5C_2 induced 42.6% and 60.7% greater signal drop at 4 and 24 h time points, respectively. After the 24 h imaging, we sacrificed the animals and performed Prussian blue staining with the tumor sections. In parallel to the in vivo observations, we found many areas of positive staining in the RGD-Fe_5C_2 group, but few were present in the Fe_5C_2 group (Figure 4b). To further elucidate the targeting mechanism, we also performed Prussian blue and integrin β_3 double staining with tumors from the RGD-Fe_5C_2 group (Figure 4b). We observed overall good overlap between the two stainings, confirming that the tumor targeting was mediated by RGD-integrin interactions. The distribution of RGD-Fe_5C_2 nanoparticles among major organs was also studied by Positive Prussian blue staining, which found many iron deposits in the liver and spleen. This is mainly attributed to the uptake by the Kupffer cells and macrophages as part of the reticuloendothelial system (RES) intervention (Figure 4c), though body iron stores may have contributed to a certain level.[18a] As expected, few particles were found in other major organs such as the lung, kidneys, and brain.

Though an ancient material, the uses of Fe_5C_2 in a biological setting have seldom been exploited. The current study offers the first investigation in this regard. The in vitro, in vivo, and pathological studies suggest the great potential of Fe_5C_2 nanoparticles for bio-applications. Despite the promise, however, more studies are needed to fully understand and optimize this new type of biomaterial. First, systematic toxicity studies are needed. Though relative low cytotoxicity was observed in the current study, the metabolism and long-term impact of Fe_5C_2 nanoparticles within a biological system is largely unknown and needs thorough investigations. In one pilot study, we incubated Fe_5C_2 nanoparticles in a pH 5.0 buffer solution. After 72 h, it was found that most of the nanoparticles were partially or completely degraded (Figure S2). It is therefore believed that, similar to iron oxides, Fe_5C_2 can be degraded in an acidic lysosome environment, releasing Fe to join the body iron stores. Second, it is worthwhile to explore the impact of particle size on the magnetic properties, cellular uptake, in vivo circulation half-lives, bio-distribution, and targeting selectivity of Fe_5C_2 nanoparticles. An increased particle size may lead to higher magnetization and r_2 relaxivity, but may also cause a shorter circulation time and a higher level of RES uptake. Balance has to be struck to achieve the best performance. Third, the surface coating may affect the pharmacokinetics of nanoparticles and is worthy of optimization. In the current study, a PEGylated phospholipid was used as the coating. Other coating materials such as silica,[20] dopamine derivatives,[5,21] and tri-block co-polymers[18b] are also expected to be able to modify Fe_5C_2 nanoparticles. Fourth, as a proof-of-concept investigation, this study chose RGD as a tumor targeting ligand. In future investigations, it is important to evaluate performance of Fe_5C_2 nanoparticles when conjugated with different targeting motifs. Ultimately, there are many other potential applications with Fe_5C_2 nanoparticles. These include liver and lymph node imaging for which iron oxide nanoparticles are dominantly used. Moreover, with a high magnetism, Fe_5C_2 nanoparticles also hold promise in magnetic separation/purification, drug delivery,

gene transfection, cell tracking, and magnetic hyperthermia. [1b,22] The related investigations are underway.

Supplementary Material

Refer to Web version on PubMed Central for supplementary material.

Acknowledgements

This work was supported by an NCI/NIH R00 grant (5R00CA153772, J. X.), University of Georgia Faculty Research Grant (Q.Z.), and NSFC (51125001, 51172005, 90922033).

References

[1]. a)Xie J, Liu G, Eden HS, Ai H, Che X, Acc. Chem. Res 2011, 44, 883; [PubMed: 21548618] b)Xie J, Lee S, Chen X, Adv. Drug. Delivery Rev 2010, 62, 1064.

[2]. Huang J, Zhong X, Wang L, Yang L, Mao H, Theranostics 2012, 2, 86. [PubMed: 22272222]

[3]. Jun YW, Huh YM, Choi JS, Lee JH, Song HT, Kim S, Yoon S, Kim KS, Shin JS, Suh JS, Cheon J, J. Am. Chem. Soc 2005, 127, 5732. [PubMed: 15839639]

[4]. Cheon J, Lee JH, Acc. Chem. Res 2008, 41, 1630. [PubMed: 18698851]

[5]. Peng S, Wang C, Xie J, Sun S, J. Am. Chem. Soc 2006, 128, 10676. [PubMed: 16910651]

[6]. Wang C, Peng S, Lacroix LM, Sun SH, Nano Res. 2009, 2, 380.

[7]. Peng S, Xie J, Sun S, J. Solid. State Chem 2008, 181, 1560. [PubMed: 19122843]

[8]. a)Wang C, Hou Y, Kim J, Sun S, Angew. Chem. Int. Ed 2007, 46, 6333;b)Xu C, Yuan Z, Kohler N, Kim J, Chung MA, Sun S, J. Am. Chem. Soc 2009, 131, 15346. [PubMed: 19795861]

[9]. a)Hou YL, Xu ZC, Peng S, Rong CB, Liu JP, Sun SH, Adv. Mater 2007, 19, 3349;b)Xu C, Xu K, Gu H, Zheng R, Liu H, Zhang X, Guo Z, Xu B, J. Am. Chem. Soc 2004, 126, 9938. [PubMed: 15303865]

[10]. Sun SH, Anders S, Thomson T, Baglin JEE, Toney MF, Hamann HF, Murray CB, Terris BD, J. Phys. Chem. B 2003, 107, 5419.

[11]. a)Gao J, Liang G, Zhang B, Kuang Y, Zhang X, Xu B, J. Am. Chem. Soc 2007, 129, 1428–1433; [PubMed: 17263428] b)Horev-Azaria L, Kirkpatrick CJ, Korenstein R, Marche PN, Maimon O, Ponti J, Romano R, Rossi F, Golla-Schindler U, Sommer D, Uboldi C, Unger RE, Villiers C, Toxicol. Sci 2011, 122, 489. [PubMed: 21602188]

[12]. Yang C, Zhao H, Hou Y, Ma D, J. Am. Chem. Soc 2012, 134, 15814. [PubMed: 22938192]

[13]. Schnepp Z, Wimbush SC, Antonietti M, Giordano C, Chem. Mater 2010, 22, 5340.

[14]. a)Hager GT, Bi XX, Derbyshire FJ, Eklund PC, Stencei JM, Abstr. Pap. Am. Chem. S 1991, 202, 101;b)Stencel JM, Eklund PC, Bi XX, Davis BH, Hager GT, Derbyshire FJ, Stud. Surf. Sci. Catal 1993, 75, 1797.

[15]. Giordano C, Kraupner A, Wimbush SC, Antonietti M, Small 2010, 6, 1859. [PubMed: 20661996]

[16]. Sun SH, Zeng H, Robinson DB, Raoux S, Rice PM, Wang SX, Li GX, J. Am. Chem. Soc 2004, 126, 273. [PubMed: 14709092]

[17]. Zhang Y, Yang Y, Cai W, Theranostics 2010, 1, 135–148.

[18]. a)Lee HY, Li Z, Chen K, Hsu AR, Xu C, Xie J, Sun S, Chen X, J. Nucl. Med 2008, 49, 1371; [PubMed: 18632815] b)Chen K, Xie J, Xu H, Behera D, Michalski MH, Biswal S, Wang A, Chen X, Biomaterials 2009, 30, 6912–6919; [PubMed: 19773081] c)Lee H, Yu MK, Park S, Moon S, Min JJ, Jeong YY, Kang HW, Jon S, J. Am. Chem. Soc 2007, 129, 12739; [PubMed: 17892287] d)Huh YM, Jun YW, Song HT, Kim S, Choi JS, Lee JH, Yoon S, Kim KS, Shin JS, Suh JS, Cheon J, J. Am. Chem. Soc 2005, 127, 12387. [PubMed: 16131220]

[19]. Yang L, Peng XH, Wang YA, Wang X, Cao Z, Ni C, Karna P, Zhang X, Wood WC, Gao X, Nie S, Mao H, Clin. Cancer Res. 2009, 15, 4722. [PubMed: 19584158]

[20]. Pinho SL, Pereira GA, Voisin P, Kassem J, Bouchaud V, Etienne L, Peters JA, Carlos L, Mornet S, Geraldes CF, Rocha J, Delville MH, ACS Nano 2010, 4, 5339. [PubMed: 20795638]

[21]. Zhao Z, Zhou Z, Bao J, Wang Z, Hu J, Chi X, Ni K, Wang R, Chen X, Chen Z, Gao J, Nat. Commun 2013, 4, 2266. [PubMed: 23903002]

[22]. Yu MK, Park J, Jon S, Theranostics 2012, 2, 3. [PubMed: 22272217]

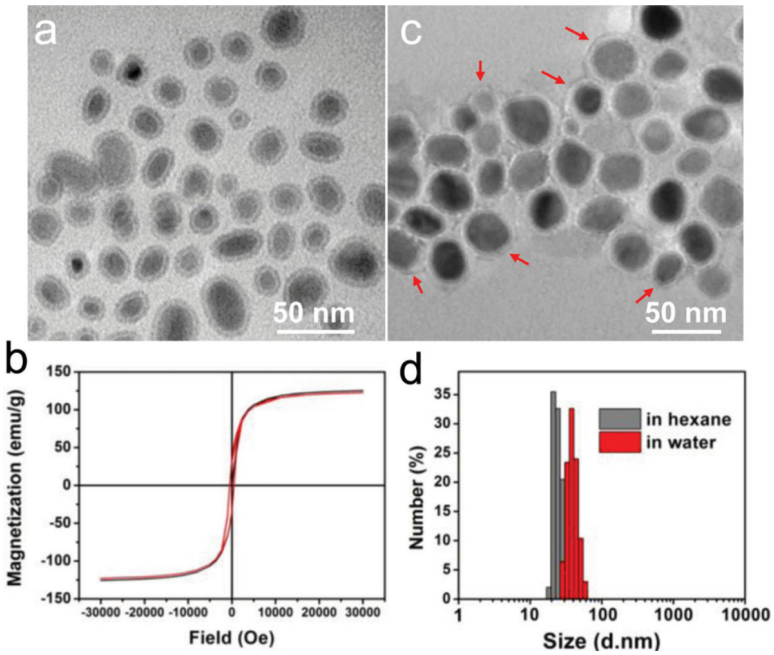

Figure 1.

a) TEM image of as-synthesized Fe_5C_2 nanoparticles in hexane. (b) Hysteresis loops of Fe_5C_2 nanoparticles that were as-synthesized (black curve) and after exposure to the air for one week (red curve). The two curves were almost identical, suggesting good stability of the nanoparticles. No remnant magnetization and coercivity were observed, indicating that they were superparamagnetic at room temperature. The Ms values were determined to be 125.4 and 122.6 emu/g, respectively, for as-synthesized Fe_5C_2 nanoparticles and those after one week aging. c) TEM image of DSPE-PEG-COOH coated Fe_5C_2 nanoparticles in water. The red arrows point to the DSPE-PEG-COOH coating that is manifested as dim halos surrounding the particles. d) The hydrodynamic sizes of Fe_5C_2 nanoparticles are ~22 and ~35 nm, respectively, before and after the DSPE-PEG-COOH coating. The results correlate well with the TEM observations.

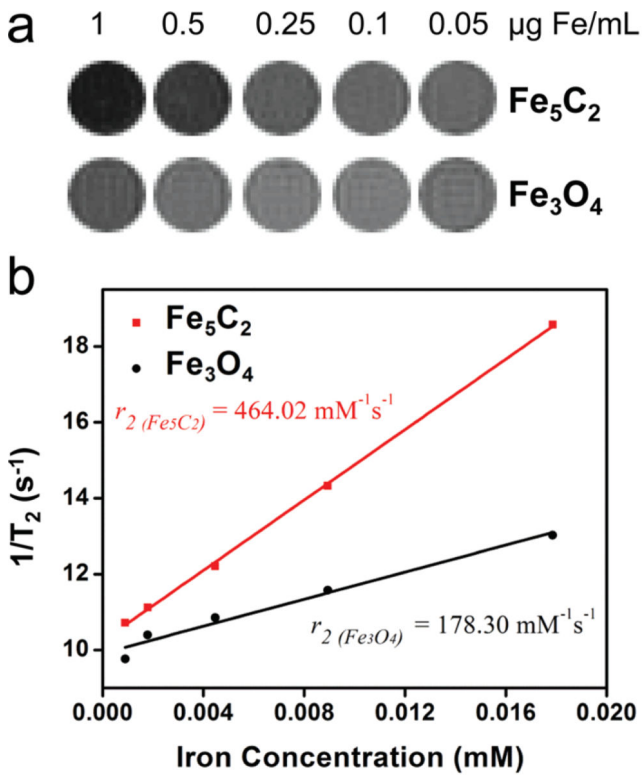

Figure 2.

a) Phantom studies with Fe_5C_2 and Fe_3O_4 nanoparticles dispersed in 1% agarose gel at different concentrations on a 7T magnet. Fe_5C_2 nanoparticles induced more significant signal drop than Fe_3O_4 nanoparticles at the same Fe concentrations. b) r_2 relaxivities derived from the imaging results in a). Fe_5C_2 nanoparticles have an r_2 of 464.02 $mM^{-1}s^{-1}$ (R^2 = 0.9995) compared to that of 178.30 $mM^{-1}s^{-1}$ (R^2 = 0.9758) for Fe_3O_4 nanoparticles.

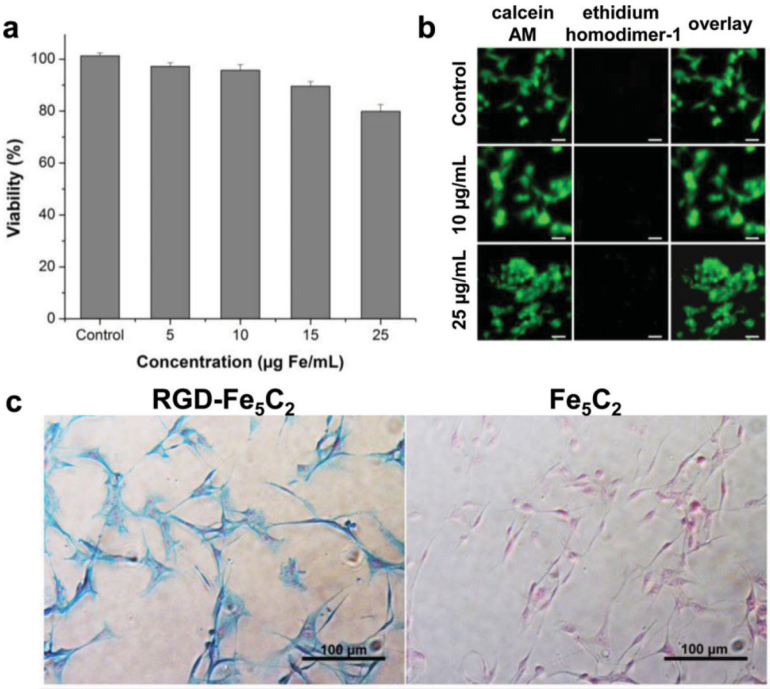

Figure 3.

a) MTT assays with Fe_5C_2 nanoparticles on U87MG cells. The cells retained over 80% viability in the tested concentration range (0 – 25 μg Fe/mL). b) Live/dead assays with Fe5C2 nanoparticles on U87MG cells. No red fluorescence (ethidium homodimer-1) was observed in the tested concentration range (0 – 25 μg Fe/mL). c) Cellular uptake studies with U87MG cells. The cells were incubated with either RGD-Fe_5C_2 or Fe_5C_2 nanoparticles (5 μg Fe/mL) for 1h, and then subjected to Prussian blue staining. Positive staining was found with almost all the cells when RGD-Fe_5C_2 nanoparticles were used. On the contrary, Fe_5C_2 nanoparticles showed little cellular uptake.

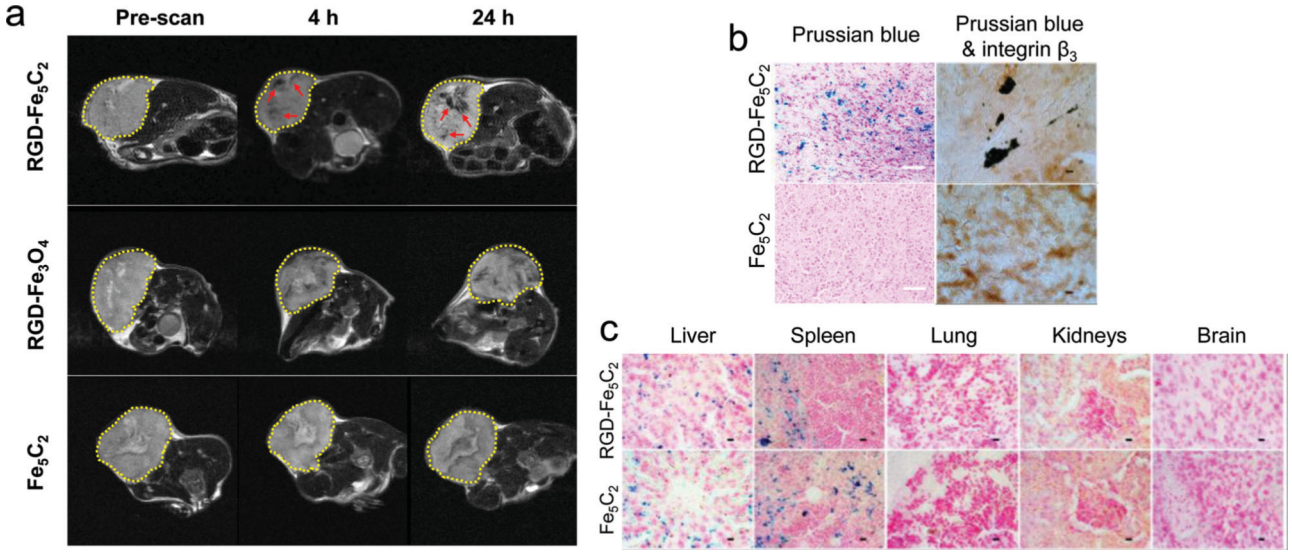

Figure 4.

a) MR imaging results. U87MG tumor bearing mice were intravenously injected with RGD-Fe_5C_2, RGD-Fe_3O_4, or Fe_5C_2 nanoparticles (10 mg Fe/kg). Scans were performed before, and 4 and 24 h after the administration. In both the RGD-Fe_5C_2 and RGD-Fe_3O_4 groups, black areas (in the RGD-Fe_5C_2 group highlighted by red arrows) were found distributed in the tumors (circled by yellow dotted lines). RGD-Fe_5C_2 induced more significant signal drop than RGD-Fe_3O_4 at both time points. b) Left column: Prussian blue staining with tumor tissues. Positive staining was found in the RGD-Fe_5C_2 group but not in the Fe_5C_2 group. Scale bars, 50 μm. Right column: Prussian blue and integrin β_3 double staining with the tumor tissues. Good overlap was observed in the RGD-Fe_5C_2 group, indicating that the tumor accumulation was mainly caused by RGD-integrin interactions. Scale bars, 10 μm. c) Prussian blue staining with tissue samples from the liver, spleen, lung, kidneys, and brain. Particles were accumulated in the liver and spleen but not in the other major organs. Scale bars, 10 μm.